Multifractality in plasma edge electrostatic turbulence

C. Rodrigues Neto,[1,a)] Z. O. Guimarães-Filho,[2] I. L. Caldas,[2] I. C. Nascimento,[2] and Yu. K. Kuznetsov[2]
[1]*GRIFE-Escola de Artes, Ciências e Humanidades Universidade de São Paulo, Brazil*
[2]*Instituto de Física, Universidade de São Paulo, Brazil*

(Received 9 June 2008; accepted 30 July 2008; published online 19 August 2008)

Plasma edge turbulence in Tokamak Chauffage Alfvén Brésilien (TCABR) [R. M. O. Galvão *et al.*, Plasma Phys. Contr. Fusion **43**, 1181 (2001)] is investigated for multifractal properties of the fluctuating floating electrostatic potential measured by Langmuir probes. The multifractality in this signal is characterized by the full multifractal spectra determined by applying the wavelet transform modulus maxima. In this work, the dependence of the multifractal spectrum with the radial position is presented. The multifractality degree inside the plasma increases with the radial position reaching a maximum near the plasma edge and becoming almost constant in the scrape-off layer. Comparisons between these results with those obtained for random test time series with the same Hurst exponents and data length statistically confirm the reported multifractal behavior. Moreover, the persistence of these signals, characterized by their Hurst exponent, present radial profile similar to the deterministic component estimated from analysis based on dynamical recurrences.
© *2008 American Institute of Physics*. [DOI: 10.1063/1.2973175]

I. INTRODUCTION

The knowledge of the electrostatic plasma turbulence in the tokamak (specifically, in the region comprising the outer portion of the plasma column and the region that separates it from the vessel wall) is essential to improve the plasma confinement.[1–3] Thus, several properties of the turbulent fluctuations have been investigated. Similarities of these properties in different devices have been found through different kinds of numerical analyses.[4–9]

Quantitative investigations of the electrostatic fluctuations using spectral approaches like Fourier and wavelet analysis show that drift waves are destabilized in the confining magnetic field so as to yield a turbulent spectrum.[1,10–12] On the other hand, dynamical diagnostics used to describe fluid turbulence[13] have been applied to analyze the plasma edge turbulence, as the return-time statistics[8,14] and recurrence analyses.[15]

Furthermore, the structure of intermittent plasma signals can be studied using techniques as volatility clustering, fat tails, and long-range correlations.[4,5] Some of the methods to characterize the long-range correlations from experimental time series are the autocorrelation functions, power spectral densities, and probability distribution functions (PDFs).[5–7,16]

Monofractal characteristics of the electrostatic fluctuations in plasmas can be determined by means of the Hurst exponents,[7,16] which reveal that these fluctuations are persistent. In addition, multifractal analyses provide further insights on the self-affine scaling exponents. Moreover, these analyses, performed by structure functions (SFs) and wavelet transform modulus maxima (WTMM) methods show that these fluctuations are multifractal[16–19] and their multiscale nature is associated with the presence of different kinds of structures in the plasma edge.[18,19] The experimental signals commonly used in these fractal analyses are the local density and turbulent flux for which fat tails were clearly observed.[6,7] Therefore, several investigations present evidence of multifractality in these signals, but for the fluctuating floating potential there is less evidence of this behavior.

In tokamak Chauffage Alfvén Brésilien (TCABR), multifractal behavior for the density fluctuations has also been found, similar to results observed in other tokamaks.[9] In this work we analyze the multifractal properties of fluctuating floating electrostatic potential (ϕ) measured by Langmuir probes at the plasma edge of TCABR. By applying the WTMM method we show the multifractal behavior present in these fluctuations and its nonuniformity; i.e., its dependence on the radial position. Moreover, the Hurst exponent shows a peaked radial profile with a maximum value of ~ 0.85 located near the plasma radius (at $r/a \sim 1.05$), indicating a persistent fluctuation in this region. The importance of this noticeable result should be emphasized by remembering that the recurrence plot analyses of these fluctuations show a similar radial profile determinism with a maximum in the same region.[15] These profiles' similarity may indicate that these two properties found by different dynamical methods require a common dynamic explanation.

The paper is organized as follows. In Sec. II we describe the experimental setup and present some statistical properties related to the estimated probability distribution functions (PDFs) and the moments' radial dependence of the floating electrostatic potential ϕ. Section III explains the multifractal concept and introduces the WTMM method used to distinguish the multifractal character of the experimental signal ϕ from a set of fractal test signals. The radial profiles of the multifractal spectrum parameters are discussed in the Sec. IV. Finally, in the last section we present our conclusions.

a)Electronic mail: camiloneto@usp.br.

 © 2008 American Institute of Physics

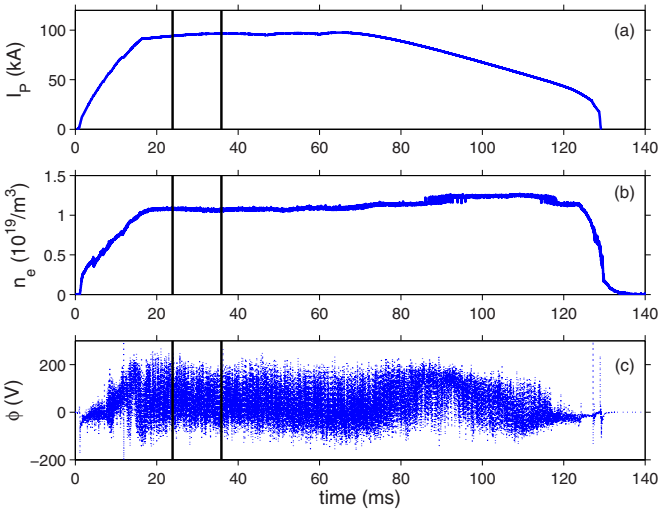

FIG. 1. (Color online) Time evolution of plasma discharge in TCABR tokamak. (a) Plasma current, (b) central chord plasma mean density, and (c) floating electrostatic potential ϕ for a typical discharge at $r/a=1$. The vertical black lines indicate the time interval analyzed.

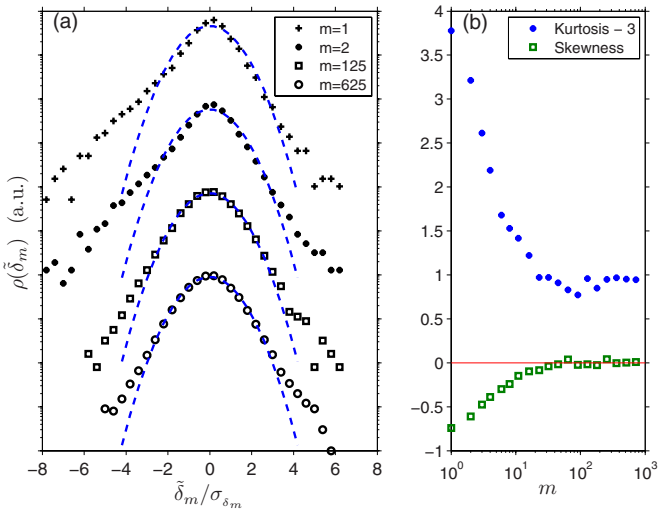

FIG. 2. (Color online) (a) PDFs of the differences, $\delta_m(t)=\phi(t+m)-\phi(t)$, for the floating electrostatic potential ϕ for different scales m at $r/a=1.17$. Dots represent experimental data and the lines are Gaussian fits. The PDFs were vertical shifted for comparison. (b) Kurtosis and skewness dependence with scale m.

II. PLASMA EDGE ELECTROSTATIC TURBULENCE IN TCABR

A. The experimental setup

The experiments analyzed in this work were performed in a hydrogen circular plasma in the Brazilian tokamak TCABR[20] (major radius $R=61$ cm and minor radius $a=18$ cm). The plasma current reaches a maximum value of 100 kA, with duration 100 ms, the hydrogen filling pressure is 3×10^{-4} Pa, and toroidal magnetic field $B_T=1.1$ T. The floating potential was measured by two Langmuir probes, poloidally separated by 0.4 cm. The probes are mounted on a movable shaft that can be displaced radially from $r=15$ to 23 cm, with respect to the center of the plasma column. In this work we shall focus on the range from 16.5 to 21 cm so as to cover both the plasma edge and the so-called scrape-off layer (SOL), the latter comprising part of the vacuum layer existing between the plasma column and the vessel wall.

The probe displacement, however, occurs only for separate discharges, in order not to disturb the plasma due to the movement of the probe. The measurements were performed at a sampling frequency of 1 MHz, and the measuring circuit has a 300 kHz bandwidth to avoid aliasing, such that in every discharge up to 10^5 points can be recorded.[12,21] Figure 1 shows the typical time evolution of a plasma discharge in TCABR. The plasma current Fig. 1(a) grows rapidly in the first 20 ms and reaches a plateau where the current stays at a 100 kA level, decaying slowly after that. The electron density evolution, indicated by Fig. 1(b), exhibits a similar evolution, with a plateau level of $n_e\sim10^{19}$ m^{-3}. The signals we are particularly interested in studying are the floating electrostatic potential ϕ, a representative example being depicted by Fig. 1(c), which shows highly irregular fluctuations. All analyzed data were chosen during the plasma current plateau in equal time intervals like the one represented by the window indicated by vertical lines in Fig. 1. We chose this window so as to avoid the discharge phase where external perturbations are usually applied for other kinds of investigations. Figure 1, however, is rather exceptional since it represents a tokamak discharge where no such perturbations have been applied to the plasma.

B. Basic statistical characterization

An intermittent fluctuation can be recognized in Fig. 1(c). A basic statistical characterization of this intermittency is presented in Figs. 2 and 3. PDFs of the differences, $\delta_m(t)=\phi(t+m)-\phi(t)$, for the floating electrostatic potential signal of Fig. 1(c) were computed for different scales m (Fig. 2). The deviation from a Gaussian distribution (skewness $S=0$ and kurtosis $K=3$) is accentuated for small scales and diminishes for large scales [Fig. 2(b)]. This behavior

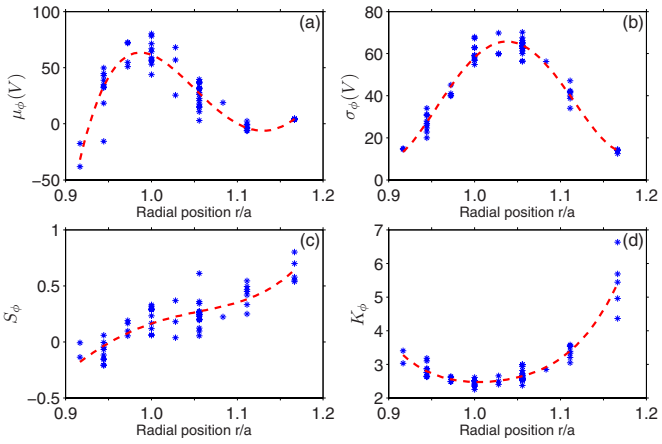

FIG. 3. (Color online) PDFs' central moments as function of the radius. The dots are for different plasma discharges and the lines are polynomial fits to guide the eyes. Plots (c) and (d) show that the PDF asymmetry and kurtosis increase to the wall.

indicates the coexistence of different characteristic scales, motivating a detailed multifractal analyses.[18,19,22]

In tokamaks, the electrostatic turbulence at the vicinity of the plasma radius shows such a significant radial dependence that even its nature may be different in the plasma edge and in the SOL. Thus, the statistical properties of the floating electrostatic potential depend on the radial location where the probe is placed. This dependence can be seen in Fig. 3 for the floating electrostatic potential radial profiles of some signal statistical parameters: mean (a), standard deviation (b), skewness (c), and kurtosis (d). Each profile of Fig. 3 contains points obtained from different discharges and the lines were obtained from polynomial fits. The mean value of ϕ presents a peak near the plasma radius, inside the plasma, with a nonuniform standard deviation with a peak just outside the plasma. So, at the plasma edge, the standard deviation is comparable to the mean value, indicating a high turbulence level in this region. In this region, according to Figs. 3(c) and 3(d), the fluctuation distribution shows a skewness and a kurtosis values that are not much different from those obtained for a Gaussian distribution ($S=0$, $K=3$). In fact, in the vicinity of the plasma radius, i.e., $r/a\sim 1$, the kurtosis is slighted lower than 3, indicating a low contribution of the extreme events. However, outside the plasma there is a tendency of S and K to increase with the distance from the plasma limiter. Thus, Fig. 3 confirms that the turbulence behavior changes significantly with the radial position in the region where the probe measurements are done.

To improve the understanding of the turbulence in this region, in the following we introduce the wavelet transform modulus maxima (WTMM) technique commonly used to perform the multifractal analysis, and finally, we apply the WTMM method to obtain the associated multifractal spectrum and its radial dependence.

III. MULTIFRACTAL ANALYSIS

The multifractal scaling analysis has been used largely in the study of turbulence of fluids[23] and, more recently, also in plasma turbulence.[18] A first access to the multifractal scaling can be done using the structure function (SF) analysis. The SFs are defined in the following way:[24]

$$S_q(Y,\tau) \equiv \langle |Y(t+\tau) - Y(t)|^q \rangle \propto \tau^{qh(q)}, \tag{1}$$

where $Y(t)=\Sigma_{t'=1}^{t}\phi(t')$, τ is the scale of analysis and $\langle\cdots\rangle$ denotes the ensemble average. A signal that is scale invariant and self-similar is said to be a fractal if the exponent $h(q)$, in Eq. (1), has the same value for all q. Otherwise, if $h(q)$ varies with q, then the signal is said to be multifractal.[25,26] When $q=2$ the SF is the correlation function; otherwise, it can be regarded as a generalization of the correlation functions. Also for $q=2$, we obtain the Hurst exponent $H=h_2$, originally defined from R/S analysis.[27] One way to interpret the Hurst exponent in a physical sense is by comparison with its values expected for known signals, for instance, the *fractional Brownian motion*.[26,28] The fractional Brownian motion can be classified following the probabilities of its fluctuations: the usual Brownian motion, obtained from the integration of a Gaussian distributed white noise, has the same probability of having positive or negative fluctuations and has $H=0.5$. A fractional Brownian motion with $H<0.5$ is more likely to have the next fluctuation with opposite sign of the last one—it is said to be antipersistent. Conversely, a fractional Brownian motion with $H>0.5$ is more likely to have the next fluctuation with the same sign of the last one—it is said to be persistent. Antipersistent signals have more local fluctuations and seem to be more irregular in small scales. Their variance diverges with time slower than the variance of the persistent signals. The latter ones fluctuate on larger scales and seem to be smoother. This discussion is done in Ref. 29 and a similar but more detailed interpretation is given in Ref. 30.

The scaling exponent h is known as the Hölder exponent and, although it can be computed using the structure function approach,[24] this method has the disadvantage of not being able to obtain the scalings of the negative moments. To obtain the full multifractal spectrum, i.e., positive and negative q moments, we make use of the wavelet transform Modulus maxima (WTMM).[31,32] The wavelet transform of a signal $X(t)$ is defined as

$$T_\psi(\tau,b_0) = \frac{1}{\tau}\sum_{t=1}^{N} X(t)\psi^*\left(\frac{t-b_0}{\tau}\right), \tag{2}$$

where $\tau>0$ is the scale being analyzed, ψ is the mother wavelet, and N is the number of discretized time steps. We used the nth-derivative of Gaussian (DOGn), whose wavelet transform has n vanishing moments and removes polynomial trends of order $n-1$ from the signal. Because the scaling properties of the signal are preserved by the wavelet transform, it is possible to obtain its multifractal spectrum using this method. The number of vanishing moments for the wavelet basis used in this paper was $n=2$.

The statistical scaling properties of the singular measures found in time series are characterized by the singularity spectrum, $D(h)$, of the Hölder exponents (h) obtained with the WTMM method[31,32] by the following equations:

$$h(q) = \lim_{\tau\to 0}\frac{1}{\ln\tau}\sum_{\{b_i(\tau)\}}\hat{T}_\psi[q;\tau,b_i(\tau)]\ln|T_\psi[\tau,b_i(\tau)]|, \tag{3}$$

$$D(h) = \lim_{\tau\to 0}\frac{1}{\ln\tau}\sum_{\{b_i(\tau)\}}\hat{T}_\psi[q;\tau,b_i(\tau)]\ln|\hat{T}_\psi[q;\tau,b_i(\tau)]|, \tag{4}$$

where

$$\hat{T}_\psi[q;\tau,b_i(\tau)] = \frac{|T_\psi[\tau,b_i(\tau)]|^q}{\Sigma_{\{b_i(\tau)\}}|T_\psi[\tau,b_i(\tau)]|^q}, \tag{5}$$

and the summing is over the set of the WT modulus maxima[33] at scale τ, $\{b_i(\tau)\}$. The singularity spectrum $D(h)$ and the Hölder exponents h are obtained from the scaling range on the linear-log plots of Eqs. (3) and (4). The whole procedure is now a standard[29] and, for brevity, it is not repeated here.

Figure 4 shows the multifractal spectra for two different radial positions: inside the plasma ($r/a=0.92$) and in the

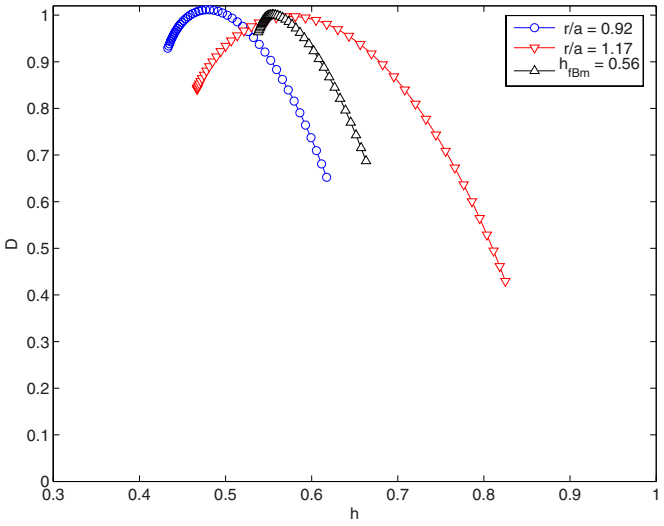

FIG. 4. (Color online) Multifractal spectrum $D(h)$ of Hölder exponent h for $r/a=0.92$ and $r/a=1.17$. For comparison, the multifractal spectrum for a fractal Brownian motion is also shown, with $h=0.56$ and with the same length of the experimental signal.

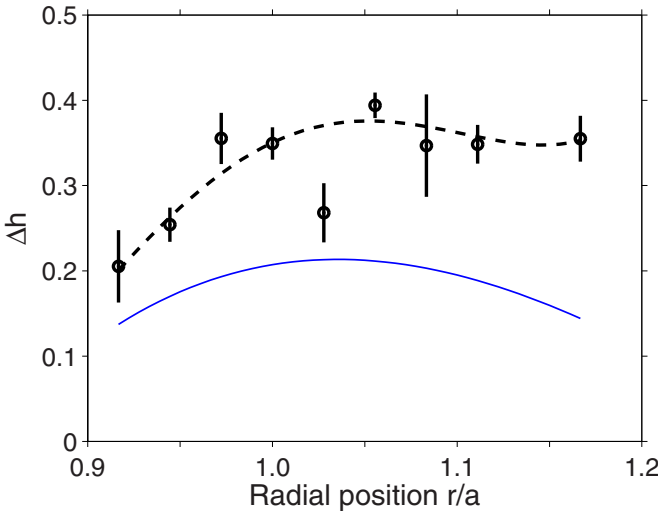

FIG. 6. (Color online) Radial profile of the multifractal spectrum width. The dotted line is a polynomial fit to indicate the average behavior. For comparison, the continuous line represents the same for ten realizations of fBm series with the same length. Experimental and fBm series were normalized to zero mean and unit standard deviation before obtaining the multifractal spectrum width.

scrape-off layer ($r/a=1.17$). For sake of comparison, it also shows a multifractal spectrum for a fractal Brownian motion (fBm) signal of the same length: as expected, this fractal signal does not show a single point spectrum, since finite effects are expected. The next section shows the radial dependence of the multifractal spectrum.

IV. MULTIFRACTAL SPECTRUM RADIAL PROFILES

In the previous section, we utilized the WTMM approach to identify the multifractal character of the floating electrostatic potential ϕ. Now we will look for the multifractal properties of the system dynamics as a function of the radius r.

The multifractal spectrum may be represented by its Hölder exponents h at their extrema points; i.e., its minima on the left (h_l) and on the right (h_r), as well as on the maximum (top), h_0, shown in Fig. 5. In Figs. 5(a)–5(c) the dots correspond to values obtained from each of two probes in 57 plasma discharges. The mean values obtained from the values shown in Figs. 5(a)–5(c), for each radial position, are represented in Fig. 5(d) with error bars corresponding to the estimated standard deviation of the mean (standard deviation over square root of the number of values). It worth noting that the point h_l shows the scaling of the large fluctuations on the time series, while the h_r captures the scaling of the small fluctuations. Moreover, the multifractality is higher for wider spectrum; i.e., for bigger differences between h_r and h_l.

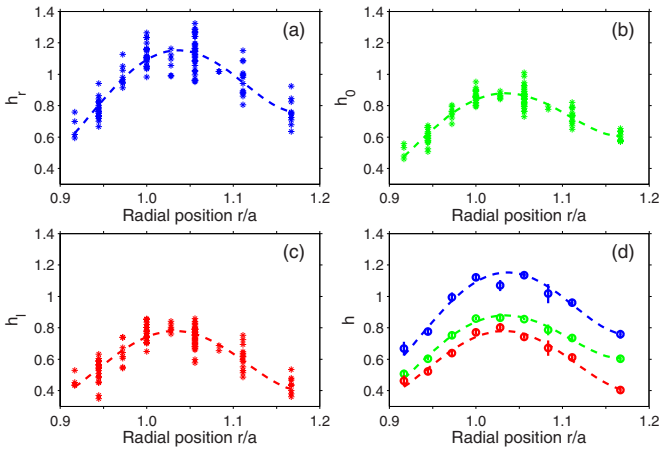

FIG. 5. (Color online) Multifractal spectrum dependence with r. The dots in the plots (a), (b), and (c) are from two probes for 57 plasma discharges. The error bars in the plot (d) are the estimated uncertainties of the mean values obtained from all analyzed plasma discharges.

The multifractal character of the time series is more evident from the plot for the spectrum width as a function of r, shown in Fig. 6. This figure shows the difference between the maximum and the minimum values of h, (h_r-h_l), for each value of r, for all the radii studied. For intermediary values of r, the multifractal spectrum gets wider, a sign of multifractality, and maintains this multifractal dynamics for higher radii. Also, the experimental signal spectrum width is wider than the monofractal fBm, plotted as a continuous line, statistically confirming its multifractality. Thus, as it can be recognized in Figs. 5 and 6, for the smallest value of r measured, the system dynamics is almost fractal, with $h_0 \sim 0.5$, a value characteristic of a random Brownian walk, as was already expected, since the time series for ϕ are almost Gaussian (see Fig. 3) at that r value.

Another representative point of the multifractal spectrum is the Hurst exponent, obtained from h_2. The radial profile of this exponent is show in Fig. 7(a). We see that the Hurst exponent presents a continuous peaked radial profile with a maximum value ~ 0.85 near the plasma radius (at $r/a \sim 1.05$). At this position the floating potential is clearly persistent while at smallest and highest r the Hurst exponent is close to 0.5, the value expected for Brownian random walks. However, according to Fig. 6, at the scrape-off layer $(r/a>1)$ the multifractality is higher than inside the plasma

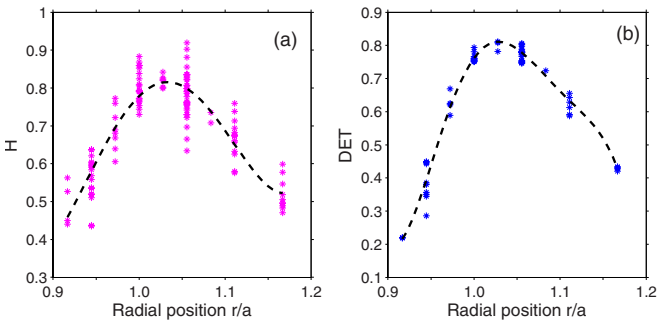

FIG. 7. (Color online) Radial profiles of (a) the Hurst exponent and (b) the deterministic character of the time series from the recurrent plot analysis (Ref. 15). The dots represent data from 57 different plasma discharges and the lines are polynomial fits to guide the eyes.

$(r/a<1)$, besides the similar persistence interpretation inferred from Fig. 7(a).

At this point, it is interesting to compare the results shown in Fig. 7(a) with that obtained for the same data in another analysis based on the recurrence quantification analysis (RQA). The RQA is a dynamical tool introduced to quantify the recurrent structures in a given time series. For a time series sampled at equally spaced time intervals $x_i=x(t=ih)$, and its embedding series $\vec{X}_i=x_i,x_{i+\tau},\ldots,x_{i+(d-1)\tau}$, where d is the embedding dimension and τ is the time delay, it is possible to obtain recurrence plots (RPs). These RPs are graphical representations of the matrix[15,34] $R_{i,j}=\Theta(\varepsilon-\|\vec{X}_i-\vec{X}_j\|)$, $i,j=1,2,\ldots,N$, where ε is the threshold, $\Theta(.)$ is the unit step function, $\|\cdots\|$ stands for the Euclidean norm, and N is the total number of points. The RP is thus obtained by assigning a black (white) dot to the points for which $R_{i,j}=1(0)$. The many kinds of structures present in a recurrence plot are used to characterize the dynamical properties of the underlying time series.[34] One measure of these structures is the determinism (DET), i.e., the fraction of recurrence points belonging to diagonal lines, which are structures parallel to the main diagonal line. Along a diagonal line, two pieces of a trajectory undergo for a certain time (the length of the diagonal) a similar evolution and visit the same region of phase space at different times. Hence the existence of many diagonal lines is a signature of determinism. The quantity DET is related with the predictability of the dynamical system, because a random process would have a recurrence plot with almost only single dots and very few diagonal lines, whereas a deterministic process has a recurrence plot with very few single dots but many long diagonal lines.

Thus, we perform this analysis to estimate the radial profile of the floating potential determinism using the DET. Figure 7(b) shows the DET radial profile (chosen values required to perform the RQA analysis are the same as those used in Ref. 15). The obtained profile has a maximum near the plasma radius $(r/a\sim1.05)$, indicating a large deterministic turbulence component in this region.

Comparing the results shown in Figs. 7(a) and 7(b), we identify that the Hurst exponent and DET have similar radial profiles. Thus, following the interpretation of these profiles, we conjecture that the persistence and the determinism may be associated to a common dynamical property that could be identified in a proper turbulence theory. Therefore, it seems worthwhile to try to identify this dynamical property in the models that describe plasma edge turbulence.

V. CONCLUSION

The focus of this work was to detect the multifractal character of the floating electrostatic potential at the TCABR plasma edge and to characterize its radial dependence. We started obtaining the radial dependence of the statistical moments, which shed some light on the plasma nonuniformities and pointed the non-Gaussian behavior of the fluctuating potential on small scales.

Using the wavelet transform modulus maxima approach, we compared the width of the multifractal spectrum of the analyzed signals with that of the fractional Brownian motion signals, to conclude positively towards the multifractal character of the fluctuating potential. We also obtain the multifractal spectrum dependence on the radial position. Finally, we show that the persistence radial profile is similar to the profile of the determinism obtained from recurrent plots analysis in a previous work.[15]

The approach presented in this paper can be followed to evaluate the dynamical models used to describe plasma edge turbulence in tokamaks. Namely, these models should reproduce the reported radial dependence of the fractality and recurrence observed in the turbulence signals.

[1] C. W. Horton, Rev. Mod. Phys. **71**, 735 (1999).
[2] A. J. Wootton, S. C. McCool, and S. Zheng, Fusion Technol. **19**, 973 (1991).
[3] F. Wagner, and U. Stroh, Plasma Phys. Controlled Fusion **35**, 1321 (1993).
[4] B. A. Carreras, B. van Milligen, M. A. Pedrosa, R. Balbín, C. Hidalgo, D. E. Newman, E. Sánches, M. Frances, I. García-Cortés, J. Bleuel, M. Endler, S. Davies, and G. F. Matthews, Phys. Rev. Lett. **80**, 4438 (1998).
[5] B. Ph. van Milligen, S. Sánchez, B. A. Carreras, V. E. Lynch, B. La Bombard, M. A. Pedrosa, C. Hidalgo, B. Gonçalves, R. Balbín, and The W7-AS Team, Phys. Plasmas **12**, 052507 (2005).
[6] G. Y. Antar, S. I. Krasheninnikov, P. Devinck, R. P. Doerner, E. M. Hollmann, J. A. Boedo, S. C. Luchardt, and R. W. Conn, Phys. Rev. Lett. **87**, 065001 (2001).
[7] Y. H. Xu, S. Jachmich, R. R. Weynants, and the TEXTOR Team, Plasma Phys. Controlled Fusion **47**, 1841 (2005).
[8] M. S. Baptista, I. L. Caldas, M. V. A. P. Heller, A. A. Ferreira, R. D. Bengtson, and J. Stöckel, Phys. Plasmas **8**, 4455 (2001).
[9] V. P. Budaev, S. A. Grashin, G. S. Kirnev, B. V. Kuteev, Yu. K. Kuznetsov, Z. O. Guimarães-Filho, I. C. Nascimento, I. L. Caldas, R. M. O. Galvão, M. P. Gryaznevich, and G. van Oost, *Europhysics Conference Abstracts, 34th EPS Conference on Plasma Physics*, Warsaw, 2007, edited by P. Gasior and J. Wolowski (European Physical Society, Mulhouse, France, 2007), Vol. 31F, P-1.088.
[10] C. Riccardi, D. Xuantong, M. Salierno, L. Gamberale, and M. Fontanesi, Phys. Plasmas **4**, 3749 (1997).
[11] A. M. Batista, I. L. Caldas, S. R. Lopes, R. L. Viana, W. Horton, and P. Morrison, Phys. Plasmas **13**, 042510 (2006).
[12] A. A. Ferreira, M. V. A. P. Heller, and I. L. Caldas, Phys. Plasmas **7**, 3567 (2000).
[13] P. Holmes, J. L. Lumley, and G. Berkooz, *Turbulence, Coherent Structures, Dynamical Systems and Symmetry* (Cambridge University Press, Cambridge, 1996).
[14] A. A. Ferreira, M. V. A. P. Heller, M. S. Baptista, and I. L. Caldas, Braz. J. Phys. **32**, 1 (2002).
[15] Z. O. Guimarães-Filho, I. L. Caldas, R. L. Viana, J. Kurths, I. C. Nascimento, and Yu. K. Kuznetsov, Phys. Lett. A **372**, 1088 (2008).
[16] Y. H. Xu, S. Jachmich, R. R. Weynants, A. Huber, B. Unterberg, and U. Samm, Phys. Plasmas **11**, 5413 (2004).
[17] B. A. Carreras, V. E. Lynch, D. E. Newman, R. Balbín, J. Bleuel, M. A.

Pedrosa, M. Endler, B. van Milligen, E. Sánchez, and C. Hidalgo, Phys. Plasmas **7**, 3278 (2000).
[18]V. P. Budaev, S. Takamura, N. Ohno, and S. Masuzaki, Nucl. Fusion **46**, S181 (2006).
[19]V. P. Budaev, Y. Kikuchi, Y. Uesugi, and S. Takamura, Nucl. Fusion **44**, S108 (2004).
[20]R. M. O. Galvão, V. Bellintani, Jr., R. D. Bengtson, A. G. Elfimov, J. I. Elizondo, A. N. Fagundes, A. A. Ferreira, A. M. M. Fonseca, Y. K. Kuznetsov, E. A. Lerche, I. C. Nascimento, L. F. Ruchko, W. P. de Sá, E. A. Saettone, E. K. Sanada, J. H. F. Severo, R. P. da Silva, V. S. Tsypin, O. C. Usuriaga, and A. Vannucci, Plasma Phys. Controlled Fusion **43**, A299 (2001).
[21]A. A. Ferreira, M. V. A. P. Heller, I. L. Caldas, E. A. Lerche, L. F. Ruchko, and L. A. Baccala, Plasma Phys. Controlled Fusion **46**, 669 (2004).
[22]V. P. Budaev, Phys. Lett. A **344**, 299 (2004).
[23]U. Frisch, *Turbulence* (Cambridge University Press, Cambridge, 1995).
[24]C. X. Yu, M. Gilmore, W. A. Peebles, and T. L. Rhodes, Phys. Plasmas **10**, 2772 (2003).
[25]G. Paladin and A. Vulpiani, Phys. Rep. **156**, 147 (1987).
[26]J. Feder, *Fractals* (Plenum, New York, 1988).
[27]M. Gilmore, C. X. Yu, T. L. Rhodes, and W. A. Peebles, Phys. Plasmas **9**, 1312 (2002).
[28]B. Mandelbrot and J. van Ness, SIAM Rev. **10**, 422 (1968).
[29]K. Bube, C. Rodrigues Neto, R. Donner, U. Schwarz, and U. Feudel, J. Phys. D **39**, 1405 (2006).
[30]J. B. Cromwell, W. C. Labys, and E. Kouassi, Empir. Econ. **25**, 563 (2000).
[31]J. Muzy, E. Bacry, and A. Arneodo, Phys. Rev. Lett. **67**, 3515 (1991).
[32]A. Arneodo, E. Bacry, and J. Muzy, Physica A **213**, 232 (1995).
[33]C. Torrence and G. P. Compo, Bull. Am. Meteorol. Soc. **79**, 61 (1998).
[34]N. Marwan, M. C. Romano, M. Thiel, and J. Kurths, Phys. Rep. **438**, 237 (2007).